

## Article

# Low-Complexity Three-Dimensional AOA-Cross Geometric Center Localization Methods via Multi-UAV Network

Baihua Shi <sup>1</sup>, Yifan Li <sup>1</sup>, Guilu Wu <sup>2</sup>, Riqing Chen <sup>3</sup>, Shihao Yan <sup>4</sup> and Feng Shu <sup>1,2,\*</sup><sup>1</sup> School of Electronic and Optical Engineering, Nanjing University of Science and Technology, Nanjing 210094, China<sup>2</sup> School of Information and Communication Engineering, Hainan University, Haikou 570228, China<sup>3</sup> Digital Fujian Institute of Big Data for Agriculture, Fujian Agriculture and Forestry University, Fuzhou 350002, China; riqing.chen@fafu.edu.cn<sup>4</sup> School of Science and Security Research Institute, Edith Cowan University, Perth, WA 6027, Australia

\* Correspondence: shufeng@hainanu.edu.cn

**Abstract:** The angle of arrival (AOA) is widely used to locate a wireless signal emitter in unmanned aerial vehicle (UAV) localization. Compared with received signal strength (RSS) and time of arrival (TOA), AOA has higher accuracy and is not sensitive to the time synchronization of the distributed sensors. However, there are few works focusing on three-dimensional (3-D) scenarios. Furthermore, although the maximum likelihood estimator (MLE) has a relatively high performance, its computational complexity is ultra-high. Therefore, it is hard to employ it in practical applications. This paper proposed two center of inscribed sphere-based methods for 3-D AOA positioning via multiple UAVs. The first method could estimate the source position and angle measurement noise at the same time by seeking the center of an inscribed sphere, called the CIS. Firstly, every sensor measures two angles, the azimuth angle and the elevation angle. Based on that, two planes are constructed. Then, the estimated values of the source position and the angle noise are achieved by seeking the center and radius of the corresponding inscribed sphere. Deleting the estimation of the radius, the second algorithm, called MSD-LS, is born. It is not able to estimate angle noise but has lower computational complexity. Theoretical analysis and simulation results show that proposed methods could approach the Cramér–Rao lower bound (CRLB) and have lower complexity than the MLE.

**Keywords:** UAV; 3-D; angle of arrival; center of inscribed sphere

**Citation:** Shi, B.; Li, Y.; Wu, G.; Chen, R.; Yan, S.; Shu, F. Low-Complexity Three-Dimensional AOA-Cross Geometric Center Localization Methods via Multi-UAV Network.

*Drones* **2023**, *7*, 318. <https://doi.org/10.3390/drones7050318>

Academic Editors: Sai Huang, Guan Gui, Xue Wang, Yuanyuan Yao and Zhiyong Feng

Received: 10 April 2023

Revised: 6 May 2023

Accepted: 10 May 2023

Published: 12 May 2023



**Copyright:** © 2023 by the authors. Licensee MDPI, Basel, Switzerland. This article is an open access article distributed under the terms and conditions of the Creative Commons Attribution (CC BY) license (<https://creativecommons.org/licenses/by/4.0/>).

## 1. Introduction

Source localization has attracted much attention for decades. In recent years, it has been used in many new applications, such as wireless sensor networks (WSN), the Internet of Things (IoT), and unmanned aerial vehicles (UAV) localization [1–3]. It is worth noting that integrated sensing and communications (ISAC) is regarded as a key technology in 6G and demands higher requirements [4]. Therefore, source localization will be a hot research topic in the future of wireless communications. As presented in [5], high-precision localization is essential in many scenarios and use cases, such as vehicle positioning in vehicle-to-everything (V2X) networks, fall detection in smart homes, drone swam synthetic aperture radar (SAR) imaging in remote sensing, user tracking in cellular networks, and so on. As a promising unified waveform in ISAC, orthogonal time frequency space (OTFS) modulation also demands accurate locations of mobile users. In addition, as massive multiple-input, multiple-output (MIMO) became widespread in all equipment, it is easy to achieve high-precision angle information. Thus, the angle of arrival (AOA) has become popular in recent years.

In the literature, there are two kinds of passive wireless signal positioning algorithms [6]. The first kind is called scene analysis. It needs to know the channel state information (CSI) of all cells in advance. Then, the source can be located by matching the

received CSI with the CSI in the database. Thus, there is an offline training phase in this system [6]. That means its accuracy is related to training. In the other words, once there is a significant change in the surrounding scene, these methods are unable to estimate the location of the source. However, these methods are low-cost and can be used in non-line-of-sight (NLOS) conditions. Thus, they are mainly employed in indoor positioning, such as fingerprint-based methods [7].

The second kind of localization method is triangulation. Time of arrival (TOA), the time difference of arrival (TDOA) [8–12], received signal strength (RSS) [13–17], and AOA [2,18,19] all fall into this category. These kinds of methods measure some physical variables related to the source location first, such as the strength of the received wireless signals, the time it takes the signal to travel from the source to the receiver, and the angle of signals emitted from the source. Therefore, these systems can be used to estimate the source position through received real-time information and can be used in both indoor and outdoor environments. Among them, the TDOA is a modified version of the TOA. The famous global positioning system (GPS) locates the source by adopting TOA. In [20], the authors focused on 2-D positioning. The maximum likelihood estimator (MLE) for RSS, TOA, and AOA was derived. Furthermore, estimator accuracy was also presented. Two bias-reduction methods were proposed in [11] to improve the accuracy. To provide guidance, the performance of the TDOA in multi-satellite localization was analyzed in [21]. In sensors that can only be equipped with one antenna, RSS is the lowest-cost scheme. Thus, many RSS-based algorithms have been studied for practical applications, such as cellular location [13], UAV localization [17], and so on.

Different from TOA, which requires accurate time synchronization between sensors, and RSS, which is sensitive to the differences in the antenna patterns of all sensors, the AOA just needs sensors to be equipped with multiple antennas, which is not a threshold to the development of MIMO. In practical applications, UAV networks will first detect a target. Then, the angles can be measured by direction of arrival (DOA) estimation [22–24]. In [22], the authors investigate DOA estimation in hybrid analog and digital (HAD) structures. Three conventional beamforming-based methods and a multiple signal classification (MUSIC)-based method are proposed to eliminate the angle ambiguity caused by the HAD structure. In order to accelerate the process of ambiguity elimination in [22], a fast elimination method was proposed in [23]. Considering that the power consumption and circuit cost is more and more unacceptable in massive MIMO, the authors adopted low-resolution ADCs for DOA estimation. Furthermore, they analyzed the performance and energy efficiency of the DOA estimation in a low-resolution architecture. In [25], polarized massive MIMO is adopted, which is considered to be a promising solution to millimeter-wave (mmWave) communication systems. In [26], the authors integrated decoupled atomic norm minimization (D-ANM) into 2-D harmonic retrieval techniques for multiple measurement vectors (MMV). This algorithm is gridless and can achieve high computational efficiency.

After collecting DOAs from all sensors, the AOA is able to be conducted. There are many closed-form estimators for 2-D AOA [18,27–32] and a few methods for 3-D scenarios [2,19,33–35]. Two MLE-based algorithms were studied in [27]. The authors proved that the proposed location-penalized MLE has higher performance in real-world experiments. In [29], a novel AOA-based source localization estimator was developed for wideband signals. The corresponding CRLB was also derived as a benchmark. To address the AOA-based self-localization problem, several efficient closed-form methods resorting to auxiliary variables were proposed in [31]. However, 2-D approaches cannot be applied to 3-D scenes. In [33], a closed-form, three-dimensional AOA was presented. It has less computational requirements than MLE by adopting instrumental variables. A noisy approximation of MLE was shown in [34]. To reduce the bias in that estimator, the authors employed weighted instrumental variables and bias compensation. In addition, the bias of sensors was not considered in most existing works. Thus, a bias-free, closed-form algorithm for 3-D AOA was proposed in [2]. Moreover, the corresponding Cramér–Rao lower bound (CRLB) was derived to provide a reference. In [19], the authors pointed out

that the hybrid Bhattacharyya–Barankin (HBB) bound is more suitable than CRLB for use as a benchmark when the noise level is high. A hybrid AOA-TDOA positioning estimator was also proposed. In addition, when the source is far enough away, the scene is considered far-field, and AOA positioning will convert to a DOA estimation. In [35], a novel 3-D AOA method for UAV positioning was proposed by adopting bistatic MIMO radar. A transmitting and receiving array measured the 2-D angle-of-departure and angle-of-arrival, respectively. Then, the 3-D position of the UAV was calculated using these angles.

The comparison of the advantages and disadvantages between three methods is listed in Table 1. A perfect omnidirectional antenna is unavailable in practice. Furthermore, antenna patterns are becoming more and more nonuniform as the development of modern communications continues. Thus, the measurement noise of RSS is high in many applications. It will be hard to employ RSS in the future due to its unsatisfactory performance. It is also difficult to obtain high-accuracy positioning with TOA because the speed of light is too fast and it is impossible to equip every sensor with an atomic clock, which is very expensive. With the rapid development of massive MIMO, it is common for sensors to be equipped with multiple antennas. Thus, we can achieve high-precision angles to serve the AOA positioning. In addition, the measurement of the angle can be taken during wireless communications. Thus, it has a relatively low communication cost. Therefore, AOA location has been adopted in Bluetooth technology and has the potential to provide sensing ability for multi-UAV networks, 6G, and other applications in the future. Moreover, there will definitely be an LOS and almost no NLOS when AOA is employed in UAVs. This condition guarantees the high accuracy angle information for source positioning by using multiple UACVs.

**Table 1.** Comparison of different localization methods.

Methods	Advantages	Disadvantages
RSS	1. Low circuit cost 2. Easy to be implemented	Performance is easily influenced by electromagnetic energy
TOA	1. The speed of light is fixed 2. Interfered with by the structure of array	Requires ultra-high-precision time measurement synchronization accuracy
AOA	Relatively low communications cost	Multiple antennas are essential

For a multi-UAV network, all UAVs should detect the source firstly. Then, DOA estimation is performed to achieve the angle in every UAV [36]. Given the source is moving, the time synchronization method should be conducted in UAVs, like time synchronous protocol for sensor networks (TPSN) [37] and reference broadcast synchronization (RBS) [38]. In addition, all UAVs should send the measured angles and location to a host UAV or a master control computer [39], where positions of UAVs could be achieved by GPS or other position system. Finally, the location of the source is estimated in the master control computer by AOA. However, we focused on the method itself and detailed implementation of hardware will be our future work.

AOA positioning is a suitable and promising location algorithm for a multi-UAV network to locate the signal source. Moreover, existing high-performance estimators for 3-D AOA localization have relatively high computational complexity, which is hard to adapt to UAVs. Although the proposed method in [2] was able to achieve a good trade-off between performance and computational complexity, it requires a prior knowledge of noise variance and a rough location, which is unavailable in practical applications. Thus, in this paper, we aim to develop high-performance and low-complexity 3-D AOA methods for source positioning using a multi-UAV network with no prior knowledge that strikes a better balance. The main contributions of this paper are summarized as follows:

1. Three-dimensional AOA positioning is considered in this paper. Inspired by the inscribed sphere of a tetrahedron, we extend every angle to a plane. Then, the 3-D

AOA localization can be used to seek out the centers of inscribed spheres for these multiple planes. Our method can not only accurately estimate the source position and the noise level at the same time, but it also has very low computational complexity, which is similar to the conventional least square (LS) estimator.

2. To further reduce computational complexity, the estimation for variance of angle noise is removed. Then, the second algorithm is born. This algorithm is based on the sum of the minimum squared distance from the estimated point to all planes. The original optimization problem can be converted to a LS problem. Thus, this method has lower computational complexity due to its closed-formed solution. The simulation results show that these two methods have similar performance. Furthermore, compared with conventional LS, the proposed methods have about 8 dB of gain.
3. The CRLB and computational complexity are presented. Theoretical analysis and simulation results respectively unveiled that the performance of the proposed methods is close to CRLB and the computational complexity is reduced significantly. The proposed methods could achieve a satisfactory balance between the performance and computational complexity.

*Notations:* Throughout the paper, vectors, and matrices are denoted by  $\mathbf{x}$  and  $\mathbf{X}$  in bold typeface, while normal typeface is used to represent scalars, such as  $x$ . Signs  $(\cdot)^T$ ,  $(\cdot)^H$ ,  $|\cdot|$ , and  $\|\cdot\|$  represent transpose, conjugate transpose, modulus, and norm, respectively.  $\mathbf{I}_M$  denotes the  $M \times M$  identity matrix. Furthermore,  $\mathbb{E}[\cdot]$  represents the expectation operator, and  $\mathbf{x} \sim \mathcal{CN}(\mathbf{m}, \mathbf{R})$  denotes a circularly symmetric complex Gaussian stochastic vector with mean vector  $\mathbf{m}$  and covariance matrix  $\mathbf{R}$ .  $\hat{x}$  denotes the estimated value of  $x$ .

The rest of this paper is organized as follows. The system model of the 3-D AOA positioning for a multi-UAV network is presented in Section 2. Then, two high-performance and low-complexity methods are proposed in Section 3. The performance accuracy and computational complexity of the methods are investigated in Section 4. In Section 5, simulated and numerical results are provided to analyze the performance and convergence of the proposed methods. Finally, we present our conclusions in Section 6.

## 2. System Model

In this paper, a 3-D AOA localization system with  $M$  UAVs is considered. Every UAV is able to measure the azimuth angle and elevation angle of the signal transmitted by the source. As shown in Figure 1, the position of the source and UAVs is defined by  $\mathbf{u}_0 = [x_0, y_0, z_0]^T$  and  $\mathbf{u}_m = [x_m, y_m, z_m]^T$ ,  $m = 1, 2, \dots, M$ , respectively. For the  $m$ th UAV, the azimuth angle  $\theta_m$  and elevation angle  $\phi_m$  related to the coordinate of the UAVs and source can be expressed by

In practice, the angles estimated by UAVs contain noise. Thus, we denote azimuth angles  $\theta_r$  and elevation angles  $\phi_r$  as

$$\theta_r = \theta + \mathbf{n}_\theta \quad (1)$$

$$\phi_r = \phi + \mathbf{n}_\phi, \quad (2)$$

respectively, where  $\theta = [\theta_1, \theta_2, \dots, \theta_M]^T$  and  $\phi = [\phi_1, \phi_2, \dots, \phi_M]^T$  are true values.  $\mathbf{n}_\theta = [n_{\theta_1}, n_{\theta_2}, \dots, n_{\theta_M}]^T$  and  $\mathbf{n}_\phi = [n_{\phi_1}, n_{\phi_2}, \dots, n_{\phi_M}]^T$  are the additive zero mean Gaussian noises, where  $\mathbf{n}_\theta \sim \mathcal{CN}(0, \sigma_\theta^2 \mathbf{I}_M)$  and  $\mathbf{n}_\phi \sim \mathcal{CN}(0, \sigma_\phi^2 \mathbf{I}_M)$ .

$$\theta_m = \arctan\left(\frac{y_m - y_0}{x_m - x_0}\right), \quad (3)$$

$$\phi_m = \arctan\left(\frac{z_m - z_0}{(x_m - x_0) \cos \theta_m + (y_m - y_0) \sin \theta_m}\right) \quad (4)$$

where  $\theta_m \in (-\pi, \pi)$  and  $\theta_m \in (-\pi/2, \pi/2)$ .

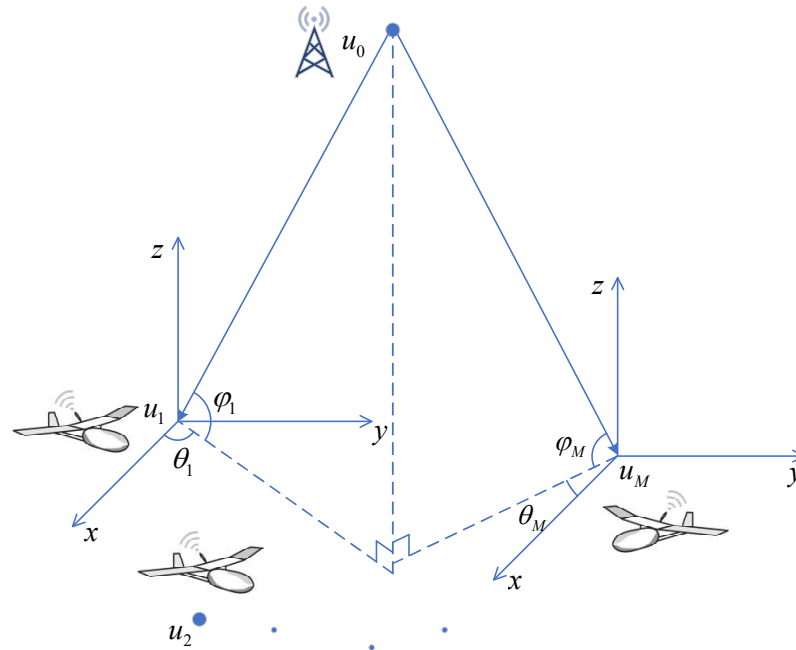


Figure 1. System model for 3-D AOA localization.

### 3. Proposed Center of Inscribed Sphere-Based Methods for AOA Localization

In this section, we integrate the idea based on the center of inscribed sphere into AOA localization, as shown in Figure 2. Two center of inscribed sphere-based methods are proposed to estimate the position of the signal.

For the  $m$ th UAV, according to (3) and the system model, the wireless signal is sent from  $u_o$  to  $u_i$ . The direction of the signal received by the  $m$ th UAV normal to the horizontal plane can be seen as a line. The plane containing this line and normal to the horizontal plane can be written as:

$$\tan \theta_m x - y - \tan \theta_m x_m + y_m = 0. \tag{5}$$

where  $x$  and  $y$  are positions of the point on the plane. Similarly, referring to (4) and the system model, we can define another plane related to  $\phi_m$ . This plane also contains the line defined by the direction of the signal. In addition, this plane is required to make an angle of  $\phi_m$  with the horizontal plane. Thus, it can be expressed as

For an arbitrary fixed point in the space, denoted by  $\tilde{\mathbf{u}} = [\tilde{x}, \tilde{y}, \tilde{z}]^T$ , the values of the Euclidean distance to the above two surfaces, (5) and (14), are given by

$$d_{m,\theta}(\tilde{\mathbf{u}}) = \frac{|\tan \theta_m \tilde{x} - \tilde{y} - \tan \theta_m x_m + y_m|}{\sqrt{(\tan \theta_m)^2 + 1}}, \tag{6}$$

and

$$d_{m,\phi}(\tilde{\mathbf{u}}) = \frac{|\tan \phi_m \cos \theta_m \tilde{x} + \tan \phi_m \sin \theta_m \tilde{y} - \tilde{z} - \tan \phi_m \cos \theta_m x_m - \tan \phi_m \sin \theta_m y_m + z_m|}{\sqrt{(\tan \phi_m \cos \theta_m)^2 + (\tan \phi_m \sin \theta_m)^2 + 1}}. \tag{7}$$

Then, to simplify the expressions of (6) and (7), let us define

$$\mathbf{a}_{m,\theta} = [\sin \theta_m, -\cos \theta_m, 0]^T \tag{8}$$

$$b_{m,\theta} = \sin \theta_m x_m - \cos \theta_m y_m \tag{9}$$

$$\mathbf{a}_{m,\phi} = [\sin \phi_m \cos \theta_m, \sin \phi_m \sin \theta_m, -\cos \phi_m]^T \quad (10)$$

$$b_{m,\phi} = \sin \phi_m \cos \theta_m x_m + \sin \phi_m \sin \theta_m y_m - \cos \phi_m z_m. \quad (11)$$

Thus, (6) and (7) can be rewritten as some direct matrix manipulations, which are given by

$$d_{m,\theta}(\tilde{\mathbf{u}}) = \left\| \mathbf{a}_{m,\theta}^T \tilde{\mathbf{u}} - b_{m,\theta} \right\| \quad (12)$$

$$d_{m,\phi}(\tilde{\mathbf{u}}) = \left\| \mathbf{a}_{m,\phi}^T \tilde{\mathbf{u}} - b_{m,\phi} \right\| \quad (13)$$

$$\begin{aligned} \tan \phi_m \cos \theta_m x + \tan \phi_m \sin \theta_m y - z \\ - \tan \phi_m \cos \theta_m x_m - \tan \phi_m \sin \theta_m y_m + z_m = 0. \end{aligned} \quad (14)$$

where  $x$ ,  $y$ , and  $z$  are the position of the point on the plane.

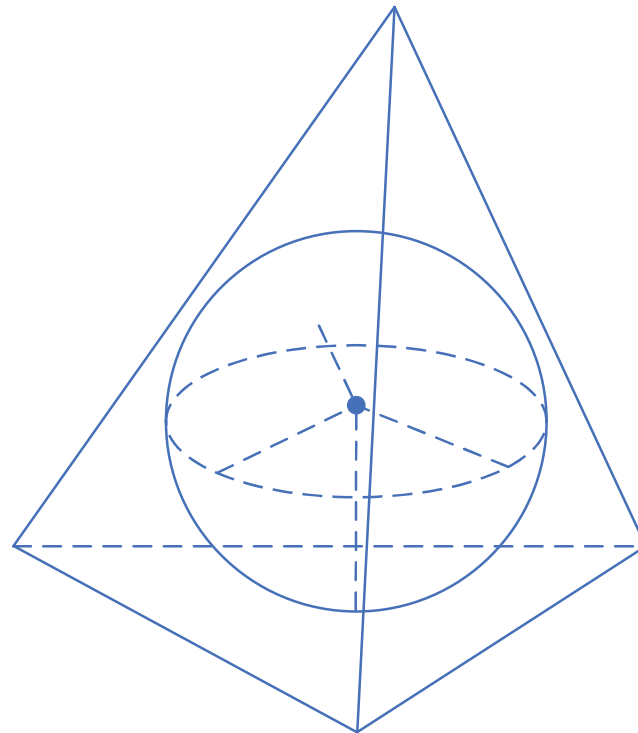


**Figure 2.** The center of inscribed sphere for a tetrahedron.

### 3.1. Proposed Center of the Inscribed Sphere Method

Let us denote the radius of inscribed sphere as  $r$ . According to the property of the inscribed sphere, distances from the center to all planes are equal to  $r$ . In other words,  $d_{m,\theta} = d_{m,\phi} = r$ ,  $m = 1, 2, \dots, M$ . To minimize the squared sum of errors, the cost function can be written as

$$\min_{\mathbf{u}, r} \sum_{m=1}^M (d_{m,\theta}(\mathbf{u}) - r)^2 + (d_{m,\phi}(\mathbf{u}) - r)^2 \quad (15)$$

Referring to [40], (15) is a nonsmooth, nonconvex problem. It is unable to be solved using conventional methods. Fortunately, the standard fixed-point (SFP) scheme, belonging to

the class of maximization–minimization approaches, is suitable for use in this case. Firstly, partial derivatives of (15) with respect to  $\mathbf{u}$  and  $r$  are given by

$$\frac{\partial f(\mathbf{u}, r)}{\partial r} = 4Mr - 2 \sum_{m=1}^M \left\| \mathbf{a}_{m,\theta}^T \mathbf{u} - b_{m,\theta} \right\| + \left\| \mathbf{a}_{m,\phi}^T \mathbf{u} - b_{m,\phi} \right\| \tag{16}$$

and

$$\begin{aligned} \frac{\partial f(\mathbf{u}, r)}{\partial \mathbf{u}} &= 2 \sum_{m=1}^M \mathbf{a}_{m,\theta} \left( \mathbf{a}_{m,\theta}^T \mathbf{u} - b_{m,\theta} \right) - r \mathbf{a}_{m,\theta} \frac{\mathbf{a}_{m,\theta}^T \mathbf{u} - b_{m,\theta}}{\left\| \mathbf{a}_{m,\theta}^T \mathbf{u} - b_{m,\theta} \right\|} \\ &+ 2 \sum_{m=1}^M \mathbf{a}_{m,\phi} \left( \mathbf{a}_{m,\phi}^T \mathbf{u} - b_{m,\phi} \right) - r \mathbf{a}_{m,\phi} \frac{\mathbf{a}_{m,\phi}^T \mathbf{u} - b_{m,\phi}}{\left\| \mathbf{a}_{m,\phi}^T \mathbf{u} - b_{m,\phi} \right\|}. \end{aligned} \tag{17}$$

Then, according to SFP, the solution of (15) can be obtained by the following iterations

$$r_{k+1} = \frac{1}{2M} \sum_{m=1}^M \left\| \mathbf{a}_{m,\theta}^T \mathbf{u}_k - b_{m,\theta} \right\| + \left\| \mathbf{a}_{m,\phi}^T \mathbf{u}_k - b_{m,\phi} \right\| \tag{18}$$

$$\mathbf{u}_{k+1} = \tilde{\mathbf{A}}^{-1} (\tilde{\mathbf{b}} + r_{k+1} \tilde{\mathbf{a}}(\mathbf{u}_k)) \tag{19}$$

where

$$\tilde{\mathbf{A}} = \sum_{m=1}^M \mathbf{a}_{m,\theta} \mathbf{a}_{m,\theta}^T + \mathbf{a}_{m,\phi} \mathbf{a}_{m,\phi}^T, \tag{20}$$

$$\tilde{\mathbf{b}} = \sum_{m=1}^M \mathbf{a}_{m,\theta} b_{m,\theta} + \mathbf{a}_{m,\phi} b_{m,\phi} \tag{21}$$

and

$$\tilde{\mathbf{a}}(\mathbf{u}) = \sum_{m=1}^M \mathbf{a}_{m,\theta} \frac{\mathbf{a}_{m,\theta}^T \mathbf{u} - b_{m,\theta}}{\left\| \mathbf{a}_{m,\theta}^T \mathbf{u} - b_{m,\theta} \right\|} + \mathbf{a}_{m,\phi} \frac{\mathbf{a}_{m,\phi}^T \mathbf{u} - b_{m,\phi}}{\left\| \mathbf{a}_{m,\phi}^T \mathbf{u} - b_{m,\phi} \right\|}. \tag{22}$$

So far,  $\mathbf{u}_0$  and  $r$  can be estimated by iteration. An initial solution can be generated by LS or a random number generator. Details about the effects of different initial solutions will be investigated in Section 5.

Let us now analyze the radius of the inscribed sphere. Given that the angle error is small, we have the following approximation:

$$\sin(\theta_m + n_{\theta_m}) \approx \sin \theta_m + n_{\theta_m} \cos \theta_m \tag{23}$$

$$\cos(\theta_m + n_{\theta_m}) \approx \cos \theta_m - n_{\theta_m} \sin \theta_m \tag{24}$$

$r$  can be expressed as

$$r = \frac{1}{2M} \sum_{m=1}^M \mathbb{E} \left[ \left\| \mathbf{a}_{m,\theta}^T \mathbf{u} - b_{m,\theta} \right\| + \left\| \mathbf{a}_{m,\phi}^T \mathbf{u} - b_{m,\phi} \right\| \right] \tag{25}$$

Thus, substituting (23) and (24) into (25), we have

$$\left\| \mathbf{a}_{m,\theta}^T \mathbf{u} - b_{m,\theta} \right\| = \left\| n_{\theta_m} ((x_0 - x_m) \cos \theta_m + (y_0 - y_m) \sin \theta_m) \right\| \tag{26}$$

Observing Figure 1, the Euclidean distance of the 2-D coordinate is introduced on the xy plane:

$$d_{xy,m} = \sqrt{(x_m - x_0)^2 + (y_m - y_0)^2} \tag{27}$$

We can thus derive a simple equation

$$\begin{aligned} (x_0 - x_m) \cos \theta_m + (y_0 - y_m) \sin \theta_m &= d_{xy,m} \cos^2 \theta_m + d_{xy,m} \sin^2 \theta_m \\ &= d_{xy,m} = d_m \cos \phi_m \end{aligned} \tag{28}$$

where  $d_m = \|u_m - u_0\|$  is the Euclidean distance from  $u_m$  to  $u_0$ . Thus, (26) could be simplified as  $\|\mathbf{a}_{m,\theta}^T \mathbf{u} - b_{m,\theta}\| = \|n_{\theta_m} d_m \cos \phi_m\|$ . Similarly,

$$\begin{aligned} &\|\mathbf{a}_{m,\phi}^T \mathbf{u} - b_{m,\phi}\| \\ &= \|n_{\phi_m} ((x_0 - x_m) \cos \theta_m \cos \phi_m + (y_0 - y_m) \sin \theta_m \cos \phi_m + (z_0 - z_m) \sin \phi_m)\| \end{aligned} \tag{29}$$

In addition, the component of (29) can also be simplified by

$$\begin{aligned} &(x_0 - x_m) \cos \theta_m \cos \phi_m + (y_0 - y_m) \sin \theta_m \cos \phi_m + (z_0 - z_m) \sin \phi_m \\ &= d_{xy,m} \cos \phi + (z_0 - z_m) \sin \phi_m = d_m \end{aligned} \tag{30}$$

Then, substituting (30) into (29), we have  $\|\mathbf{a}_{m,\phi}^T \mathbf{u} - b_{m,\phi}\| = \|n_{\phi_m} d_m\|$ . Therefore,  $r$  can be reduced to a simple form, as follows:

$$r = \frac{1}{2M} \sum_{m=1}^M \sigma_{\theta} d_m \|\cos \phi_m\| + \sigma_{\phi} d_m \tag{31}$$

It is obvious that the value of  $r$  is related to the measurement noise. Consider a special case,  $\sigma_{\theta}^2 = \sigma_{\phi}^2 = \sigma^2$ ;  $\sigma^2$  can be estimated by

$$\hat{\sigma}^2 = \frac{4M^2 r^2}{\sum_{m=1}^M d_m^2 (\cos^2 \phi_m + 1)} \tag{32}$$

Hence, this method can estimate the source location and variance of the angle measurement error at the same time. We shall call this method the center of the inscribed sphere (CIS) method.

### 3.2. Proposed Minimum Squared Distance Method

It is obvious that  $r$  could make the optimization problem complex. In addition, in many applications, it is not necessary to estimate the variance of angle measurement noise. Thus,  $r$  is useless in these applications. Moreover, considering  $\sigma_{\phi}^2 = \sigma_{\theta}^2 = 0$ , all planes will intersect at the source point. In this case,  $r = 0$ . So, we can simplify the (15) by removing  $r$ , which yields

$$\min_{\mathbf{u}} \sum_{m=1}^M d_{m,\theta}^2(\mathbf{u}) + d_{m,\phi}^2(\mathbf{u}) \tag{33}$$

Let us reduce (33) to a simple form, as follows:

$$\min_{\mathbf{u}} \|\mathbf{A}\mathbf{u} - \mathbf{b}\|^2 \tag{34}$$

where

$$\mathbf{A} = [\mathbf{A}_{\theta i}^T, \mathbf{A}_{\phi i}^T]^T \tag{35}$$

$$\mathbf{b} = [\mathbf{b}_{\theta i}^T, \mathbf{b}_{\phi i}^T]^T \tag{36}$$

where

$$\mathbf{A}_{\theta i} = [\mathbf{a}_{1,\theta}, \mathbf{a}_{2,\theta}, \dots, \mathbf{a}_{M,\theta}]^T \tag{37}$$

$$\mathbf{b}_{\theta i} = [b_{1,\theta}, b_{2,\theta}, \dots, b_{M,\theta}]^T \tag{38}$$

$$\mathbf{A}_{\phi i} = [\mathbf{a}_{1,\phi}, \mathbf{a}_{2,\phi}, \dots, \mathbf{a}_{m,\phi}]^T \tag{39}$$

$$\mathbf{b}_{\phi i} = [b_{1,\phi}, b_{2,\phi}, \dots, b_{M,\phi}]^T \tag{40}$$

Obviously, (34) is an LS problem. Hence, the solution can be given by

$$\hat{\mathbf{u}} = (\mathbf{A}^T \mathbf{A})^{-1} \mathbf{A}^T \mathbf{b} \tag{41}$$

This approach can be called the minimum squared distance-based least square (MSD-LS). Compared with CIS, this method has lower computational complexity because it directly employs LS. However,  $\mathbf{A}$  in (35) is not a noiseless matrix. In other words, both  $\mathbf{A}$  and  $\mathbf{b}$  contain measurement noise. Thus, to improve the accuracy, total least square (TLS) can be adopted.

#### 4. Analysis

In this section, we show the CRLB of the 3-D AOA and compare the computational complexity of the proposed methods with other related algorithms from the literature.

##### 4.1. Performance Accuracy

The CRLB is considered as the minimum error variance of an unbiased estimator. Therefore, we present the CRLB for the 3-D AOA as a benchmark to analyze the performance of the proposed methods. By referring to [41], the expression of CRLB is given by

$$\mathbf{CRLB} = \mathbf{F}^{-1} \tag{42}$$

where  $\mathbf{F}$  is the Fisher information matrix, which is shown as

$$\mathbf{FIM} = -\mathbb{E} \left[ \frac{\partial^2 \ln f(\boldsymbol{\theta}, \boldsymbol{\phi})}{\partial \mathbf{u} \partial \mathbf{u}^T} \right] \tag{43}$$

With the help of [2], when the covariance matrices of the angle noise are given by  $\sigma_\theta^2 \mathbf{I}_M$  and  $\sigma_\phi^2 \mathbf{I}_M$ , we can easily derive the corresponding CRLB for 3-D AOA positioning, which is given by

$$\mathbf{CRLB} = \begin{bmatrix} \sum_{m=1}^M \sigma_\theta^2 \frac{\sin^2 \theta_m}{d_m^2 \cos^2 \phi_m} + \sigma_\phi^2 \frac{\sin^2 \phi_m \cos^2 \theta_m}{d_m^2} & \sum_{m=1}^M \sigma_\theta^2 \frac{\sin^2 \phi_m \sin \theta_m \cos \theta_m}{d_m^2} - \sigma_\phi^2 \frac{\sin \theta_m \cos \theta_m}{d_m^2 \cos^2 \phi_m^2} & -\sigma_\phi^2 \sum_{m=1}^M \frac{\sin \phi_m \cos \phi_m \cos \theta_m}{d_m^2 \cos^2 \phi_m^2} \\ \sum_{m=1}^M \sigma_\theta^2 \frac{\sin^2 \phi_m \sin \theta_m \cos \theta_m}{d_m^2} - \sigma_\phi^2 \frac{\sin \theta_m \cos \theta_m}{d_m^2 \cos^2 \phi_m^2} & \sum_{m=1}^M \sigma_\theta^2 \frac{\cos^2 \theta_m}{d_m^2 \cos^2 \phi_m} + \sigma_\phi^2 \frac{\sin^2 \phi_m \sin^2 \theta_m}{d_m^2} & -\sigma_\phi^2 \sum_{m=1}^M \frac{\sin \phi_m \cos \phi_m \sin \theta_m}{d_m^2 \cos^2 \phi_m^2} \\ -\sigma_\phi^2 \sum_{m=1}^M \frac{\sin \phi_m \cos \phi_m \cos \theta_m}{d_m^2 \cos^2 \phi_m^2} & -\sigma_\phi^2 \sum_{m=1}^M \frac{\sin \phi_m \cos \phi_m \sin \theta_m}{d_m^2 \cos^2 \phi_m^2} & \sigma_\phi^2 \sum_{m=1}^M \frac{\cos^2 \phi_m}{d_m^2} \end{bmatrix}^{-1} \tag{44}$$

In Section 5, we will compare the performance of proposed methods with other existing algorithms and adopt (44) as a benchmark.

##### 4.2. Computational Complexity

Note that values of (20) and (21) can be computed once in CIS. Thus, the computational complexity of CIS is  $\mathcal{O}(31M + 7 + 6K(M + 2))$ , where  $K$  is the number of iterations. In

other words, the initial value has an effect on the computational complexity. How to obtain a suitable initial value to achieve a relative low computational complexity will be discussed in Section 5. By employing LS, MSD-LS is also a low complexity method, and its computational complexity is  $\mathcal{O}(28M + 27)$ . The computational complexity of [2] is  $\mathcal{O}(165M + 897)$ . For the ease of comparison between different methods, the computational complexity of the proposed two methods are shown in Table 2. Meanwhile, two commonly used algorithms, LS and the MLE, are also listed for comparison. Although the MLE can approach the CRLB, its complexity grows at  $\mathcal{O}(M^3)$ . Compared with the bias reduction pseudolinear estimator (BR-PLE) in [2], when the number of iterations is over 23, the computational complexity of CIS will be higher. Conversely, CIS has lower complexity. MSD-LS needs no iteration. Thus, it always has lower complexity. The computational complexity of the two proposed algorithms is a linear function of  $M$ , which is similar to LS.

**Table 2.** Computational complexity of different methods.

Algorithms	Complexity
Conventional LS	$\mathcal{O}(23M + 27)$
MLE in [19]	$\mathcal{O}(K(27M^3 + 9M^2 + 124M + 9) + 5M)$
BR-PLE in [2]	$\mathcal{O}(165M + 897)$
Proposed CIS	$\mathcal{O}(31M + 7 + 6K(M + 2))$
Proposed MSD-LS	$\mathcal{O}(28M + 27)$

## 5. Simulation Results and Analysis

In this section, simulation results are presented to evaluate the performance of the proposed methods with existing approaches. In addition, the performance of CIS with initial values generated by different methods and iterations of CIS are presented. Then, the MSE over the number of UAVs is investigated. Finally, we analyze the iterations of the CIS method. Detailed values of simulation parameters are shown in Table 3. Mean square error (MSE) is chosen as the metric of performance, which is given by

$$MSE = \sum_{n=1}^N \|\hat{u}_n - u_0\|^2. \quad (45)$$

All simulation results are averaged over 8000 Monte Carlo simulations.

**Table 3.** Values of simulation parameters.

Parameter	Value
Source location	[25, 25, 25] m
The range of UAVs' locations	50 × 50 × 50 m
The number of UAVs	20
Angle measurement variance	−5 dB

In Figure 3, we demonstrate the MSE of different 3-D AOA methods versus the variance in the angle measurement noise. All parameters and results are shown in dB. For comparison, we consider the conventional LS in [42], MLE in [19], and BR-PLE in [2].  $\sigma^2$  increases from −20 dB to 0 dB. The MLE is almost identical to the CRLB, which is in accordance with general knowledge. Furthermore, the proposed CIS and MSD-LS methods have similar performance as BR-PLE in [2] and are able to approach the CRLB with all angle variances. In addition, compared with LS, both of the proposed methods have a gain of about 8 db. More importantly, referring to Section 4, the proposed CIS and MSD-LS methods have much less computational complexity than BR-PLE and MLE.

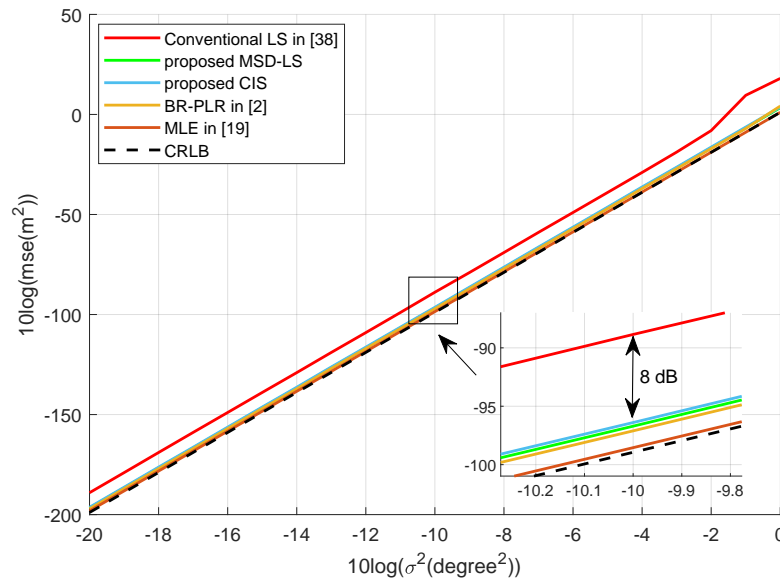


Figure 3. MSE of different AOA localization methods with different angle noise.

Figure 4 shows the MSE over the number of UAVs using different 3-D AOA methods. UAVs are randomly distributed in space. It can be seen that both of the proposed methods also have a gain of about 8 db over LS, and they have similar performance as BR-PLR in [2], and even better in certain cases. This may be because of the configuration of multiple UAV networks. An insightful observation is that the performance differences in all these methods have similar values. Especially when the number of UAVs becomes small, all of the methods approach the CRLB’s performance. To sum up, the proposed CIS and MSD-LS methods have a satisfactory performance with less computational complexity.

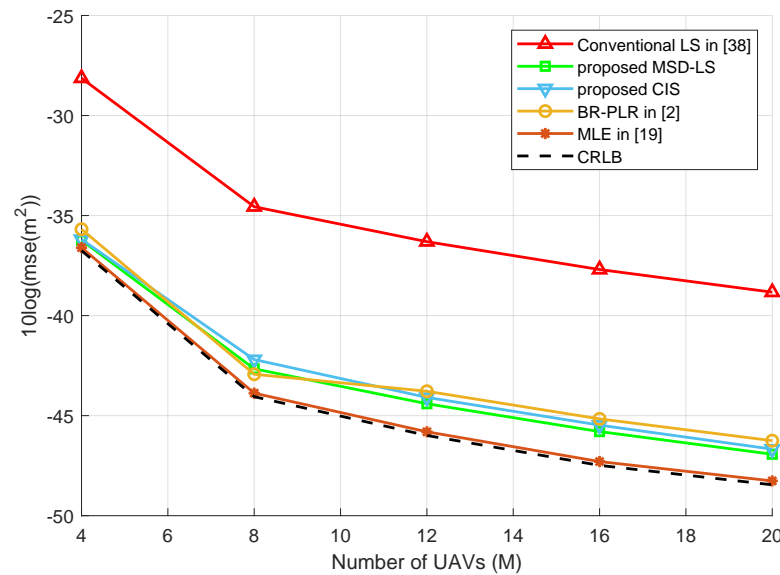
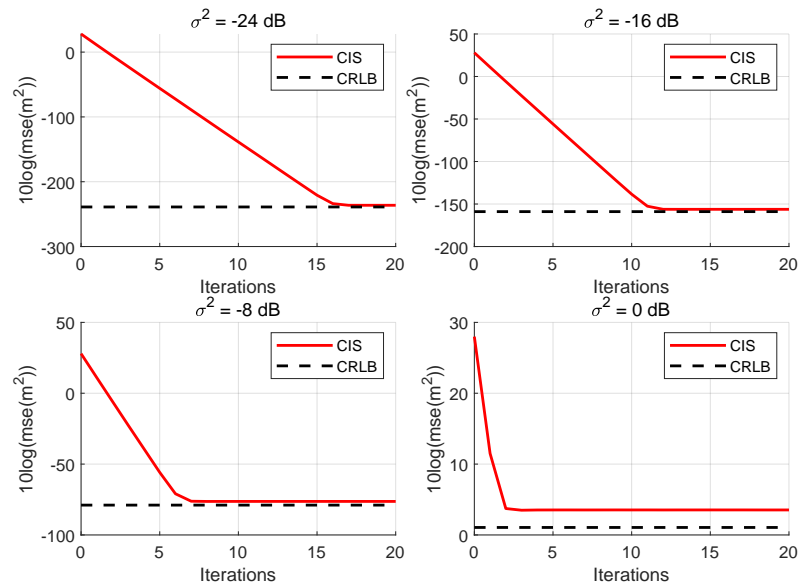


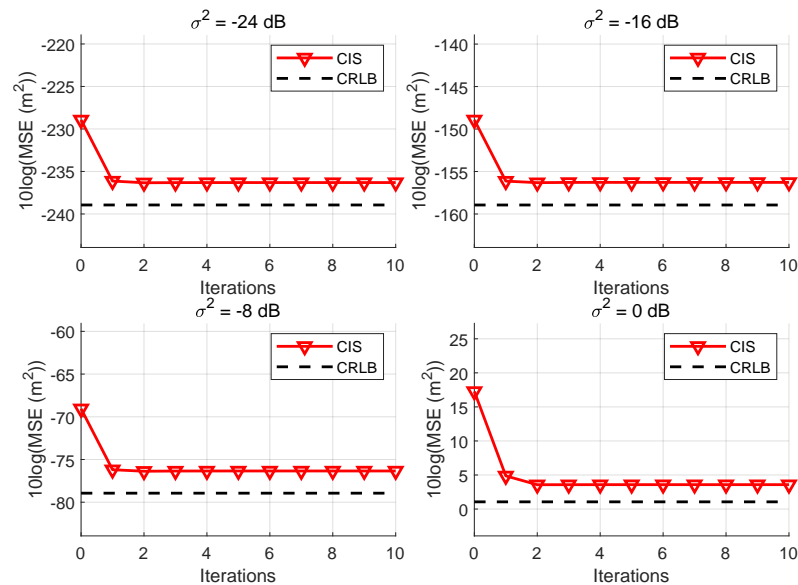
Figure 4. MSE of different AOA localization methods with different numbers of UAVs.

The MSE of the CIS method versus the number of iterations with different noise levels is plotted in Figure 5, where a random generator and conventional LS are adopted to generate an initial value in Figure 5a,b, respectively. It can be seen that CIS is convergent with any initial values in Figure 5a. Furthermore, the convergence speed is about 16.5 dB per iteration. Thus, as noise decreases, the convergence speed becomes faster. Observing Figure 5b, we find that two or three iterations are enough when LS is used. In this case,

the computational complexity is about  $\mathcal{O}(66M + 58)$ , which is faster when noise is very low. According to Table 2, when the number of iterations is greater than four, it is better to adopt LS to generate an initial solution. Therefore, random generators can be replaced by conventional LS to generate an initial value in low-noise regions. To sum up, the highest computational complexity of CIS is about  $\mathcal{O}(66M + 58)$ , which is still lower than BR-PLS in [2].



(a) An initial solution is generated by random generation



(b) An initial solution is generated by LS

Figure 5. MSE of CIS method with iterations and different angle noise levels.

### 6. Conclusions

In this work, two low-complexity, center of inscribed sphere-based approaches are proposed in a 3-D AOA model for source localization via a multi-UAV network. The location of the signal source and the angle measurement noise could be estimated at the same time using the CIS method. MSD-LS is a reduced form of CIS obtained by deleting the angle noise estimator, and it has a closed-form solution. Compared with conventional

LS, both of the proposed methods have a gain of about 8 db, which is very close to the MLE and CRLB. The computational complexity of these methods is a function of the number of UAVs,  $M$ , which is close to LS and much lower than the MLE. More importantly, our proposed methods are able to estimate the source position with no prior knowledge of angle measurement variance. What is more, when MSD-LS is employed, recursive least square can be adopted to uniformly assign computational tasks to all UAVs. Then, the multi-UAV network is able to estimate the source location independently. Therefore, our methods have the potential to be widely used in 3-D AOA localization for to locate wireless signal sources in multi-UAV networks.

**Author Contributions:** Conceptualization, B.S.; methodology, B.S.; software, B.S.; validation, B.S. and Y.L.; formal analysis, Y.L.; investigation, G.W., S.Y., R.C. and F.S.; resources, R.C.; data curation, S.Y.; writing—original draft preparation, B.S.; writing—review and editing, B.S.; visualization, B.S.; supervision, F.S.; project administration, F.S.; funding acquisition, R.C. and F.S. All authors have read and agreed to the published version of the manuscript.

**Funding:** This work was supported in part by the National Natural Science Foundation of China (Nos. U22A2002, 61972093 and 62071234), Hainan Province Science and Technology Special Fund (ZDKJ2021022), and the Scientific Research Fund Project of Hainan University under Grant KYQD(ZR)-21008.

**Data Availability Statement:** Not applicable.

**Conflicts of Interest:** The authors declare no potential conflict of interest with respect to the research, authorship, and/or publication of this article.

## Abbreviations

The following abbreviations are used in this manuscript:

3-D	Three-dimensional
UAV	Unmanned aerial vehicle
MIMO	Multiple-input, multiple-output
LOS	Line-of-sight
DOA	Directory of arrival
RSS	Received signal strength
AOA	Angle of arrival
TOA	Time of arrival
CRLB	Cramér–Rao lower bound
WSN	Wireless sensor network
MLE	Maximum likelihood estimator
IoT	Internet of Things
CSI	Channel state information
OTFS	Orthogonal time frequency space
MUSIC	Multiple signal classification
ANM	Atomic norm minimization
CIS	Center of the inscribed sphere
MSD	Minimum squared distance
BR-PLE	Bias reduction pseudolinear estimator

## References

1. Wan, P.; Huang, Q.; Lu, G.; Wang, J.; Yan, Q.; Chen, Y. Passive localization of signal source based on UAVs in complex environment. *China Commun.* **2020**, *17*, 107–116. [\[CrossRef\]](#)
2. Wang, Y.; Ho, K.C. An Asymptotically Efficient Estimator in Closed-Form for 3-D AOA Localization Using a Sensor Network. *IEEE Trans. Wirel. Commun.* **2015**, *14*, 6524–6535. [\[CrossRef\]](#)
3. Kaur, N.; Sood, S.K. An Energy-Efficient Architecture for the Internet of Things (IoT). *IEEE Syst. J.* **2017**, *11*, 796–805. [\[CrossRef\]](#)
4. Liu, F.; Masouros, C.; Petropulu, A.P.; Griffiths, H.; Hanzo, L. Joint Radar and Communication Design: Applications, State-of-the-Art, and the Road Ahead. *IEEE Trans. Commun.* **2020**, *68*, 3834–3862. [\[CrossRef\]](#)
5. Cui, Y.; Liu, F.; Jing, X.; Mu, J. Integrating Sensing and Communications for Ubiquitous IoT: Applications, Trends, and Challenges. *IEEE Netw.* **2021**, *35*, 158–167. [\[CrossRef\]](#)
6. Wu, Z.H.; Han, Y.; Chen, Y.; Liu, K.J.R. A Time-Reversal Paradigm for Indoor Positioning System. *IEEE Trans. Veh. Technol.* **2015**, *64*, 1331–1339. [\[CrossRef\]](#)
7. Le Dortz, N.; Gain, F.; Zetterberg, P. WiFi fingerprint indoor positioning system using probability distribution comparison. In Proceedings of the 2012 IEEE International Conference on Acoustics, Speech and Signal Processing (ICASSP), Kyoto, Japan, 25–30 March 2012; pp. 2301–2304.
8. Ho, K.; Chan, Y. Geolocation of a known altitude object from TDOA and FDOA measurements. *IEEE Trans. Aerosp. Electron. Syst.* **1997**, *33*, 770–783. [\[CrossRef\]](#)
9. Ho, K.C.; Lu, X.; Kovavisaruch, L. Source Localization Using TDOA and FDOA Measurements in the Presence of Receiver Location Errors: Analysis and Solution. *IEEE Trans. Signal Process.* **2007**, *55*, 684–696. [\[CrossRef\]](#)
10. Wang, G.; Chen, H. An Importance Sampling Method for TDOA-Based Source Localization. *IEEE Trans. Wirel. Commun.* **2011**, *10*, 1560–1568. [\[CrossRef\]](#)
11. Ho, K.C. Bias Reduction for an Explicit Solution of Source Localization Using TDOA. *IEEE Trans. Signal Process.* **2012**, *60*, 2101–2114. [\[CrossRef\]](#)
12. Meng, W.; Xie, L.; Xiao, W. Optimality Analysis of Sensor-Source Geometries in Heterogeneous Sensor Networks. *IEEE Trans. Wirel. Commun.* **2013**, *12*, 1958–1967. [\[CrossRef\]](#)
13. Weiss, A. On the accuracy of a cellular location system based on RSS measurements. *IEEE Trans. Veh. Technol.* **2003**, *52*, 1508–1518. [\[CrossRef\]](#)
14. Catovic, A.; Sahinoglu, Z. The Cramer-Rao bounds of hybrid TOA/RSS and TDOA/RSS location estimation schemes. *IEEE Commun. Lett.* **2004**, *8*, 626–628. [\[CrossRef\]](#)
15. Tomic, S.; Beko, M.; Dinis, R. RSS-Based Localization in Wireless Sensor Networks Using Convex Relaxation: Noncooperative and Cooperative Schemes. *IEEE Trans. Veh. Technol.* **2015**, *64*, 2037–2050. [\[CrossRef\]](#)
16. Jin, D.; Yin, F.; Fritsche, C.; Gustafsson, F.; Zoubir, A.M. Bayesian Cooperative Localization Using Received Signal Strength with Unknown Path Loss Exponent: Message Passing Approaches. *IEEE Trans. Signal Process.* **2020**, *68*, 1120–1135. [\[CrossRef\]](#)
17. Li, Y.; Shu, F.; Shi, B.; Cheng, X.; Song, Y.; Wang, J. Enhanced RSS-Based UAV Localization Via Trajectory and Multi-Base Stations. *IEEE Commun. Lett.* **2021**, *25*, 1881–1885. [\[CrossRef\]](#)
18. Lingren, A.G.; Gong, K.F. Position and Velocity Estimation Via Bearing Observations. *IEEE Trans. Aerosp. Electron. Syst.* **1978**, *AES-14*, 564–577. [\[CrossRef\]](#)
19. Wang, Y.; Ho, K.C. Unified Near-Field and Far-Field Localization for AOA and Hybrid AOA-TDOA Positionings. *IEEE Trans. Wirel. Commun.* **2018**, *17*, 1242–1254. [\[CrossRef\]](#)
20. Bishop, A.N.; Anderson, B.D.O.; Fidan, B.; Pathirana, P.N.; Mao, G. Bearing-Only Localization using Geometrically Constrained Optimization. *IEEE Trans. Aerosp. Electron. Syst.* **2009**, *45*, 308–320. [\[CrossRef\]](#)
21. Shu, F.; Yang, S.; Lu, J.; Li, J. On Impact of Earth Constraint on TDOA-Based Localization Performance in Passive Multisatellite Localization Systems. *IEEE Syst. J.* **2018**, *12*, 3861–3864. [\[CrossRef\]](#)
22. Shu, F.; Qin, Y.; Liu, T.; Gui, L.; Zhang, Y.; Li, J.; Han, Z. Low-Complexity and High-Resolution DOA Estimation for Hybrid Analog and Digital Massive MIMO Receive Array. *IEEE Trans. Commun.* **2018**, *66*, 2487–2501. [\[CrossRef\]](#)
23. Shi, B.; Jiang, X.; Chen, N.; Teng, Y.; Lu, J.; Shu, F.; Zou, J.; Li, J.; Wang, J. Fast ambiguous DOA elimination method of DOA measurement for hybrid massive MIMO receiver. *Sci. China Inf. Sci.* **2022**, *65*, 159302. [\[CrossRef\]](#)
24. Shi, B.; Chen, N.; Zhu, X.; Qian, Y.; Zhang, Y.; Shu, F.; Wang, J. Impact of Low-Resolution ADC on DOA Estimation Performance for Massive MIMO Receive Array. *IEEE Syst. J.* **2022**, *16*, 2635–2638. [\[CrossRef\]](#)
25. Wen, F.; Gui, G.; Gacanin, H.; Sari, H. Compressive Sampling Framework for 2D-DOA and Polarization Estimation in mmWave Polarized Massive MIMO Systems. *IEEE Trans. Wirel. Commun.* **2022**, *22*, 3071–3083. [\[CrossRef\]](#)
26. Zhang, Y.; Wang, Y.; Tian, Z.; Leus, G.; Zhang, G. Efficient Super-Resolution Two-Dimensional Harmonic Retrieval With Multiple Measurement Vectors. *IEEE Trans. Signal Process.* **2022**, *70*, 1224–1240. [\[CrossRef\]](#)
27. Wang, Z.; Luo, J.A.; Zhang, X.P. A Novel Location-Penalized Maximum Likelihood Estimator for Bearing-Only Target Localization. *IEEE Trans. Signal Process.* **2012**, *60*, 6166–6181. [\[CrossRef\]](#)
28. Wang, J.; Chen, J.; Cabric, D. Stansfield Localization Algorithm: Theoretical Analysis and Distributed Implementation. *IEEE Wirel. Commun. Lett.* **2013**, *2*, 327–330. [\[CrossRef\]](#)
29. Lu, L.; Wu, H.C. Novel Robust Direction-of-Arrival-Based Source Localization Algorithm for Wideband Signals. *IEEE Trans. Wirel. Commun.* **2012**, *11*, 3850–3859. [\[CrossRef\]](#)

30. Le Cadre, J.P.; Jaetffret, C. On the convergence of iterative methods for bearings-only tracking. *IEEE Trans. Aerosp. Electron. Syst.* **1999**, *35*, 801–818. [[CrossRef](#)]
31. Shao, H.J.; Zhang, X.P.; Wang, Z. Efficient Closed-Form Algorithms for AOA Based Self-Localization of Sensor Nodes Using Auxiliary Variables. *IEEE Trans. Signal Process.* **2014**, *62*, 2580–2594. [[CrossRef](#)]
32. Zhou, Q.; Duan, Z. Weighted intersections of bearing lines for AOA based localization. In Proceedings of the 17th International Conference on Information Fusion (FUSION), Salamanca, Spain, 7–10 July 2014; pp. 1–8.
33. Dogancay, K.; Ibal, G. Instrumental Variable Estimator for 3D Bearings-Only Emitter Localization. In Proceedings of the 2005 International Conference on Intelligent Sensors, Sensor Networks and Information Processing, Melbourne, VIC, Australia, 5–8 December 2005; pp. 63–68.
34. Doğancay, K. 3D Pseudolinear Target Motion Analysis From Angle Measurements. *IEEE Trans. Signal Process.* **2015**, *63*, 1570–1580. [[CrossRef](#)]
35. Wen, F.; Shi, J.; Gui, G.; Gacanin, H.; Dobre, O.A. 3-D Positioning Method for Anonymous UAV Based on Bistatic Polarized MIMO Radar. *IEEE Internet Things J.* **2023**, *10*, 815–827. [[CrossRef](#)]
36. Florio, A.; Avitabile, G.; Coviello, G. Multiple Source Angle of Arrival Estimation Through Phase Interferometry. *IEEE Trans. Circuits Syst. II Exp. Briefs* **2022**, *69*, 674–678. [[CrossRef](#)]
37. Gou, P.; Li, F.; Wang, Y.; Li, M. Low Energy Consumption and High-Precision Time Synchronization Algorithm Based on Improved TPSN in Wireless Sensor Networks. In Proceedings of the 2018 International Conference on Engineering Simulation and Intelligent Control (ESAIC), Changsha, China, 10–11 August 2018; pp. 54–57.
38. Elson, J.; Girod, L.; Estrin, D. Fine-grained network time synchronization using reference broadcasts. *ACM SIGOPS Oper. Syst. Rev.* **2002**, *36*, 147–163. [[CrossRef](#)]
39. BniLam, N.; Nasser, S.; Weyn, M. Angle of Arrival Estimation System for LoRa Technology based on Phase Detectors. In Proceedings of the 2022 16th European Conference on Antennas and Propagation (EuCAP), Madrid, Spain, 27 March–1 April 2022; pp. 1–5.
40. Palomar, D.P.; Eldar, Y.C. *Convex Optimization in Signal Processing and Communications*; Cambridge University Press: Cambridge, UK, 2010.
41. Kay, S.M. *Fundamentals of Statistical Signal Processing*; PTR Prentice Hall: Hoboken, NJ, USA, 1993.
42. Badriasl, L.; Dogancay, K. Three-dimensional target motion analysis using azimuth/elevation angles. *IEEE Trans. Aerosp. Electron. Syst.* **2014**, *50*, 3178–3194. [[CrossRef](#)]

**Disclaimer/Publisher’s Note:** The statements, opinions and data contained in all publications are solely those of the individual author(s) and contributor(s) and not of MDPI and/or the editor(s). MDPI and/or the editor(s) disclaim responsibility for any injury to people or property resulting from any ideas, methods, instructions or products referred to in the content.